



# Calculation of the Beam-Modulation Effect of the Lung in Carbon Ion and Proton Therapy With Deterministic Pencil Beam Algorithms

Toke Printz Ringbæk<sup>1,2</sup>, Alina Santiago<sup>1,2,3</sup>, Leszek Grzanka<sup>4</sup>, Kilian Baumann<sup>1,5</sup>, Veronika Flatten<sup>1,5</sup>, Rita Engenhardt-Cabillic<sup>1,3</sup>, Niels Bassler<sup>6,7,8</sup>, Klemens Zink<sup>3,5</sup> and Uli Weber<sup>9\*</sup>

<sup>1</sup>Department of Radiotherapy and Radiation Oncology, Philipps-University, Marburg, Germany, <sup>2</sup>Department of Radiotherapy, University Hospital Essen, Essen, Germany, <sup>3</sup>Department of Radiotherapy and Radiation Oncology, University Medical Center, Gießen and Marburg, Giessen, Germany, <sup>4</sup>Institute of Nuclear Physics, Polish Academy of Sciences, Krakow, Poland, <sup>5</sup>University of Applied Science, Gießen-Friedberg, Giessen, Germany, <sup>6</sup>Department of Physics, Medical Radiation Physics, Stockholm University, Stockholm, Sweden, <sup>7</sup>Department of Oncology and Pathology, Medical Radiation Physics, Karolinska Institute, Stockholm, Sweden, <sup>8</sup>Department of Experimental Clinical Oncology, Aarhus University Hospital, Aarhus, Denmark, <sup>9</sup>GSI Helmholtzzentrum für Schwerionenforschung, Darmstadt, Germany

## OPEN ACCESS

### Edited by:

Yolanda Prezado,  
INSERM U1021 Signalisation normale  
et pathologique de l'embryon aux  
thérapies innovantes des cancers,  
France

### Reviewed by:

Kevin Souris,  
Catholic University of Louvain,  
Belgium  
Urszula Jelen,  
Ingham Institute of Applied Medical  
Research, Australia

### \*Correspondence:

Uli Weber  
U.Weber@gsi.de

### Specialty section:

This article was submitted to Medical  
Physics and Imaging,  
a section of the journal  
Frontiers in Physics

**Received:** 31 May 2020

**Accepted:** 14 October 2020

**Published:** 18 November 2020

### Citation:

Ringbæk TP, Santiago A, Grzanka L,  
Baumann K, Flatten V, Engenhardt-  
Cabillic R, Bassler N, Zink K and Weber  
U (2020) Calculation of the Beam-  
Modulation Effect of the Lung in  
Carbon Ion and Proton Therapy With  
Deterministic Pencil Beam Algorithms.  
*Front. Phys.* 8:568176.  
doi: 10.3389/fphy.2020.568176

Ion beams passing through lung tissue show more pronounced energy straggling than expected for solid materials of the same thickness. Energy straggling in active scanning particle therapy can enlarge the pencil beam Bragg peaks in-depth as well as displace them, deteriorating the dose coverage of a target within the lung. While this is not yet considered in any known treatment planning system, we implement a mathematical model to be used for treatment planning, using TRiP98, which relies on a deterministic pencil beam algorithm. Through a randomization process based on a continuous Poisson probability distribution, the HU values of lung voxels are replaced with a modified value in successive iterations. The beam-modulation effect of the lung can thus be taken into account in treatment planning by recalculating the dose  $n$  times for  $n$  randomized CTs using the raster scan file of a plan that was optimized on the nonmodulated CT. The evaluation follows by averaging the resulting  $n$  dose distributions and comparing to the corresponding nonmodulated dose distribution, attending at dosimetric indices and dose-volume histograms. In this work, the functionality of these routines was tested for proton and carbon ion plans for two selected lung cancer patient cases with deep-seated tumors, showing that, with existing standard tools, it is possible to calculate the beam-modulation effect of the lung in TRiP98 in a transparent way. Variable model parameters, such as modulation power, voxel size and density voxel selection range, were evaluated. Furthermore, a systematic study for spherical geometries in a lung tissue CT cube is presented to investigate general trends.

**Keywords:** ion beam therapy, particle therapy, proton therapy, lung cancer, treatment planning, pencil beam scanning

## 1. INTRODUCTION

With the dose deposited locally in the energy-dependent narrow Bragg peak (BP) after which little-to-no-dose is given, particle therapy offers potentially more conformal treatments, as compared to photon irradiation, with improved normal tissue sparing. In particular with the pencil beam scanning method, where the lateral beam displacement is done by magnets and the range of each BP is changed by modulating the beam energy, a more conformal dose delivery, with fewer field directions, can be achieved compared to photons [1, 2].

Due to the porous nature of the lung, ion beams passing through a lung (or lung substitute material) show a more pronounced energy straggling than for solid materials [3, 4]. A substantial broadening of the BP shape has been found when irradiating lung tissue [5, 6]. So far, current treatment planning systems (TPS) assume no additional BP broadening due to tissue heterogeneities. Ordinary planning CT images cannot capture this beam-modulation effect of the lung since the CT voxel size spatially undersamples the microscopic lung alveoli. However, the beam-modulation effect of the lung could be of clinical relevance for lung tumor treatments, which motivates this study. If this broadening effect is not taken into consideration, it can potentially lead to an undesired inhomogeneity in the dose distribution, underdosage of the planning target volume (PTV) and overdosage of the healthy surrounding normal tissue, especially in the distal region close to the PTV [3, 7].

Through the use of a 3D printed binary voxel model (the voxels in the geometry are either composed by air or by the printing plastic material) the BP degradation of lung irradiation for protons has been shown to cause for initial beam energies of 140 and 200 MeV an increase of up to 60% for the 80–20% distal beam fall-off as compared to the unperturbed reference curve [5]. Using a similar binary voxel model, a mathematical method for estimating the broadening effect of a porous material has been developed [4, 6, 8]. The degree of this broadening depends on the average size of the microscopic structures as well as on the material density and thickness. For materials with a fine (< 500  $\mu\text{m}$ ) and homogeneous microscopic structure, the BP enlargement has been shown to be well-described by a modulation of the unperturbed reference Bragg curve for water with a normal distribution and its sigma as a parameter for the strength of the modulation effect.

Treatment planning studies investigating the effects on the dose uncertainties in treatment plans of lung cancer patients are limited to a few published works. Flatten et al. [9] investigated the effects of the BP degradation in proton beams by using CT phantoms with spherical targets of variable sizes placed at different depths in the lung. The lung modulation has been implemented in the TOPAS Monte Carlo tool [6] using sets of modulated DICOM images. It was shown that the underdosage of the target volume, due to the BP degradation, increases with an increasing depth of the tumor in lung and a decreasing tumor volume. In a further study by the same group [10] the effects were investigated on proton treatment plans of lung cancer patients. It was found that the maximum underdosage of the target volume due to the BP degradation was in the order of 5% while the average underdosage was roughly 2%. In another study [11] the

effects on clinical treatment plans in proton beams were investigated using an analytical approach: Instead of using sets of modulated DICOM images and Monte Carlo tools, the pristine proton BPs were convolved using the MatRad toolkit [12] with several superimposed normal distributions of sigma values defined by certain modulation power values of the lung tissue. The underdosage of the target volumes was comparable to the results from Baumann [6]. However, to the best of our knowledge, there are no studies investigating the modulation effects for treatment planning with carbon ion beams. For carbon ion beams a more pronounced modulation effect is expected, because of the much sharper carbon BPs compared to protons. The lack of a carbon ion TPS for carbon ion beams that can calculate the lung modulation effect was a main motivation for this work.

To take the lung modulation effect into account directly, the CT resolution is crucial [5]. The resolution of a clinical CT image used for treatment planning is typically around 1 mm but the biological porous structure of the lung leading to the modulation is in the  $\mu\text{m}$  range. To work with CTs with  $\mu\text{m}$  resolution, assuming such images can be obtained, would lead to an impractically large data array and time increase in the handling of the DICOM data. The method presented in this work bypasses this problem.

The aim of the present work is to show that, with existing deterministic pencil beam dose calculation algorithms like the one in TRIP98 [13–15], it is possible to calculate the beam-modulation effect of the lung tissue. Here the term, “deterministic” applies to dose calculation algorithms with analytical functions that describe a 3D pencil beam dose distribution and deliver reproducible results without random seeds. TRIP98 is a treatment planning system that was developed for research and patient treatment at the Helmholtzzentrum für Schwerionenforschung, Darmstadt, Germany (GSI). It was used to treat 440 patients during the GSI pilot project. The basic algorithms and the pencil beam model of TRIP98 were implemented into the carbon ion planning module of the Siemens Syngo PT TPS [16] that is currently used at the ion beam facilities in Heidelberg (HIT), Marburg (MIT), Shanghai (SPHIC) and Pavia (CNAO). Although we are using a deterministic pencil beam dose calculation, the results of the procedure cannot be considered entirely deterministic because the sampling of the HU values is done with random functions.

The beam-modulation effect calculation is done by implementing a mathematical model based on a continuous Poisson probability distribution within the open-source PyTRiP tool [17]. Through a randomization process, the HU value of each selected lung voxel is changed into a modified value. The lung beam-modulation effect on patient treatment plans can then be estimated by recalculating the dose  $n$  times for  $n$  randomized CTs, using raster scan files for plans optimized on nonmodulated CTs and afterward averaging the  $n$  dose distributions. Thus the result can be compared to the corresponding nonmodulated dose distribution. Using spherical PTV geometries and two selected patient cases, we evaluated a number of different model and planning parameters to show their respective relevance in terms of PTV coverage deterioration as a result of the lung modulation effect for carbon ion as well as for proton plans.

## 2. MATERIALS AND METHODS

### 2.1. Treatment Planning System TRiP98 and Python Package PyTRiP98

All treatment plans were calculated using the ion TPS TRiP98 [13–15].

In former studies [18, 19], facility-specific baseline data, including depth-dose distributions and lateral profiles, were generated with SHIELD-HIT12A [20] for both carbon ions and protons.

PyTRiP [17, 21] is an open-source python package for, among other purposes, facilitating the work with TRiP98 and with TRiP native files. PyTRiP can import, export, convert and modify such files and execute TRiP98 locally or remotely. PyTRiP enables scripting large parameter studies of treatment plans and more advanced and automatized (programmable) manipulation than what a commercial TPS usually allows. PyTRiP handles the CT and planning contour files, as well as dose cubes from calculated plans and permits extensive manipulation on these objects, making it possible to randomize  $n$  CTs, recompute a plan on each of them and average all the calculated dose cubes.

The presented concept follows Baumann et al. [6] but is done in a fully automated and integrated environment and works for a standard pencil beam algorithm.

### 2.2. Mathematical Implementation of CT Randomization

For each investigated planning case, first a treatment plan on the unmodified planning CT is calculated, producing a raster scan file for each case. Afterward, a dose recalculation, using these raster scan files, is done  $n$  times following the mathematical method described below. This is based on the “binary voxel model” for porous targets, where the target is divided into high and low density voxels, which each traversing particle will hit with probabilities of  $p$  and  $(1-p)$ , respectively, [4, 6]. The probability for hitting  $k$  voxels with high density is thus given by a binomial distribution, which, for a large number of voxels, can be approximated by a normal distribution. While this normal distribution can be subsequently used to modulate the individual PBs, here we will modify the CT voxels of a certain volume of interest (VOI), in this case the ipsilateral lung  $\text{VOI}_{\text{lung}}$ .

First the tissue density in each voxel of the CT image is calculated using the standard HU conversion table of TRiP98. Then, the voxels of  $\text{VOI}_{\text{lung}}$  (within a user-defined density range  $\rho_{\text{range}}$  from  $\rho_{\text{min}}$  to  $\rho_{\text{max}}$ ) are selected and defined as the voxels to be modulated. The modulation power  $P_{\text{mod}}$  as defined prior is a good estimation for the strength of the lung modulation effect [4, 6, 8–10] and given as a second user-defined input parameter:

$$P_{\text{mod}} = \frac{\sigma^2}{t} \quad (1)$$

with  $\sigma$  being the Gaussian sigma from the normal distribution and  $t$  the mean water-equivalent path length. The larger the value of  $P_{\text{mod}}$ , the broader the BP and the wider its distal fall-off.

Both parameters  $\rho_{\text{range}}$  and  $P_{\text{mod}}$  are discussed in more detail below and are investigated within this work.

The water-equivalent voxel length  $t = \rho_{\text{H}_2\text{O}} \cdot d$  is then calculated for each individual voxel, where  $d$  is the voxel size and  $\rho_{\text{H}_2\text{O}}$  is the water-equivalent density of the given voxel. For the case that the beam is parallel to one of the three CT axes,  $d$  is simply assigned as either  $d_x$ ,  $d_y$ , or  $d_z$ , being the voxel length in the  $x$ -,  $y$ - and  $z$ -directions, respectively. If the beam direction is oblique, then the intersection lengths through each voxel can differ much from each other. We found that for our model,  $d$  can be well described by:

$$d = \left[ \left( \frac{n_x}{d_x} \right)^{\frac{2}{3}} + \left( \frac{n_y}{d_y} \right)^{\frac{2}{3}} + \left( \frac{n_z}{d_z} \right)^{\frac{2}{3}} \right]^{\frac{3}{2}} \quad (2)$$

where  $n = (n_x, n_y, n_z)$  is the normalized direction vector parallel to the beam. This formula approximates the mean-quadratic length divided by the mean length of the intersection pieces, (averaged over many shifted beams and voxels) and was tested with a simple ray-tracing program.

In each of the  $n$  runs the following procedure is performed for all selected lung voxels. The water-equivalent path length through the voxel is randomized corresponding to  $P_{\text{mod}}$ . The first approach would be a sampling by a Gaussian distribution with a width  $\sigma = (P_{\text{mod}} \cdot d \cdot \rho_{\text{H}_2\text{O}})^{1/2}$  around the water equivalent density  $\rho_{\text{H}_2\text{O}}$  of the individual voxel. However, such a Gaussian density distribution, for voxel sizes in the millimeter range, has a relevant contribution in the negative range (for details, see Ref. 6), which must be corrected by an adapted distribution with a singular weight at  $\rho_{\text{H}_2\text{O}} = 0$ . This is in accordance to the above mentioned binary voxel model and the corresponding Poisson distribution  $P(n)$ , which describes the discrete probability distribution for hitting  $n$  non-void voxels when traversing a row of the binary voxels. However, since a discrete Poisson distribution cannot be applied here, a continuous Poisson distribution for the water-equivalent thickness  $t'$  was chosen instead:

$$P\left(t'; t, P_{\text{mod}}\right) = A_0 \delta(x) + \frac{1-A_0}{\delta} \exp\left(\frac{\log(\lambda)t'}{\delta} - \lambda - \ln\Gamma\left(\frac{t'}{\delta} + 1\right)\right) \\ \delta = \delta(t, P_{\text{mod}}); \lambda = \lambda(t, P_{\text{mod}}); A_0 = A_0(t, P_{\text{mod}}) \quad (3)$$

The delta-Dirac function  $\delta(x)$  adds the aforesaid singular weight for  $t' = 0$  (Figure 1). The gamma function replaces the factorial function normally occurring in a non-continuous Poisson distribution for non-integers in order to generalize the formula into the continuous Poisson distribution. The distribution parameters,  $\delta$ ,  $\lambda$  and  $A_0$ , depend on the nonmodulated values  $t$  and the modulation power  $P_{\text{mod}}$ . The dependencies were calculated for 30 different values for  $P_{\text{mod}}$ , from 0.1 to 0.8 mm, and for 40 different  $t$  values, from 0.1 to 2.0, and interpolation between the matrix elements in these pre-calculated matrices were used to obtain other values. The mathematical principle behind these calculations are given in the subsection below.

For the density sampling of the individual voxels with an initial density  $\rho_{\text{H}_2\text{O}}$  and (mean) size  $d$  the following density distribution is then applied:

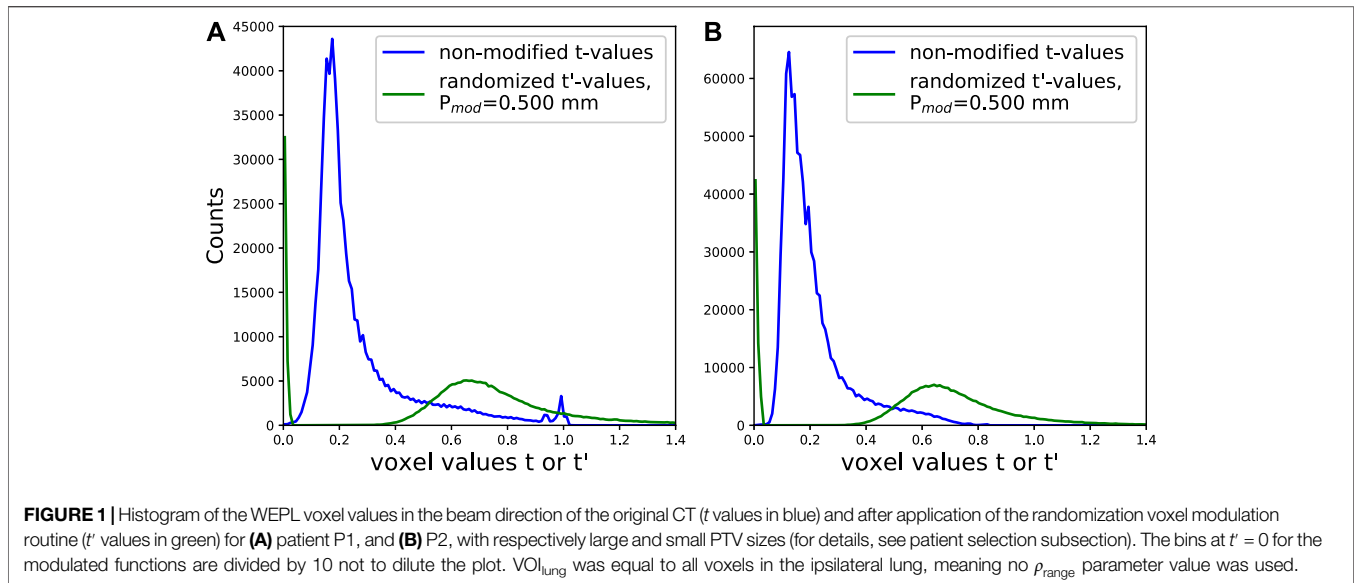


**FIGURE 1** | Histogram of the WEPL voxel values in the beam direction of the original CT ( $t$  values in blue) and after application of the randomization voxel modulation routine ( $t'$  values in green) for **(A)** patient P1, and **(B)** P2, with respectively large and small PTV sizes (for details, see patient selection subsection). The bins at  $t' = 0$  for the modulated functions are divided by 10 not to dilute the plot.  $VOI_{\text{lung}}$  was equal to all voxels in the ipsilateral lung, meaning no  $\rho_{\text{range}}$  parameter value was used.

$$\tilde{P}(\rho'_{\text{H}_2\text{O}}) = P(t' = d \cdot \rho_{\text{H}_2\text{O}}; \delta, \lambda, A_0) \quad (4)$$

At the end  $HU(\rho')$  for all selected voxels are found using the previously loaded lookup-table and a final randomized (henceforth called “modified”) CT, usable in TRiP98 for dose computation, is obtained. By recalculating the dose  $n$  times on  $n$  different modified CTs and averaging these  $n$  dose cubes, one obtains a dose distribution that takes the beam-modulation effect of the lung into account. This can then be compared to the original plan dose distribution.

In comparison to the previous work [6], where  $P(t')$  was individually optimized as a discrete function for each density value and each  $P_{\text{mod}}$ , the method presented here is much faster and can be easily reproduced with the provided tables [22]. By simultaneously calculating on 24 CPUs, for  $n = 100$ , the whole recalculation procedure lasted 15–20 min when using the TRiP dose calculation algorithm “all-point” and 50–100 min when using the more complex “multiple scattering” algorithm [23].

### 2.2.1. Calculation of the Poisson Distribution Parameters

The mathematical principle for the calculation of the tables of the Poisson distribution  $P(t')$  parameters  $\delta(t, P_{\text{mod}})$ ,  $\lambda(t, P_{\text{mod}})$  and  $A_0(t, P_{\text{mod}})$  is that these parameters were adapted such that when folding  $P(t')$   $N$  times by itself, the resulting distribution best fits the Gaussian distribution for the total path length  $N \cdot t$  and  $P_{\text{mod}}$ :

$$\begin{aligned} & \frac{P(t'; \delta, \lambda, A_0) * P(t'; \delta, \lambda, A_0) * \dots * P(t'; \delta, \lambda, A_0)}{N \text{ times}} \\ & = C \exp\left(\frac{-(t' - Nt)^2}{2\sigma^2}\right) \end{aligned} \quad (5)$$

$N$  is chosen as a value large enough (typically 10), that the contribution of the negative part of the Gaussian distribution (right term in Eq. 5) becomes negligible. The idea behind this concept is that  $P(t')$  substitutes the Gaussian distribution, avoiding non-physical negative contributions for the density distribution in the single voxels. The tables for  $\delta(t, P_{\text{mod}})$ ,  $\lambda(t, P_{\text{mod}})$  and  $A_0(t, P_{\text{mod}})$  and the scripts for their calculation can be downloaded from Mendeley [22].

### 2.2.2. Benchmark With an Analytical Convolution

Our PyTRiP routine was tested against our well-established analytical convolution method [6] (which has been confirmed experimentally [4, 8]) for 130 and 230 MeV/u carbon ion beams. For this test we used  $n = 60$ ,  $P_{\text{mod}} = 0.500$  mm and  $\rho_{\text{range}}$  from 0.1 to 0.5 g/cm<sup>3</sup> to calculate the modified doses. A lung tissue cube with constant HU of −741 HU [24] and a length of 15 cm in the beam direction was placed within a water phantom, starting at 3 cm water phantom depth  $z$ . For each depth value  $z$  of the modulated curve the pristine depth-dose curve (in water equivalent scale) was individually convoluted by a Gaussian filter, with a  $\sigma$ -value given as  $(t \cdot P_{\text{mod}})^{1/2}$ , where  $t$  is the water equivalent thickness of the lung tissue in the beam path up to the depth  $z$ .

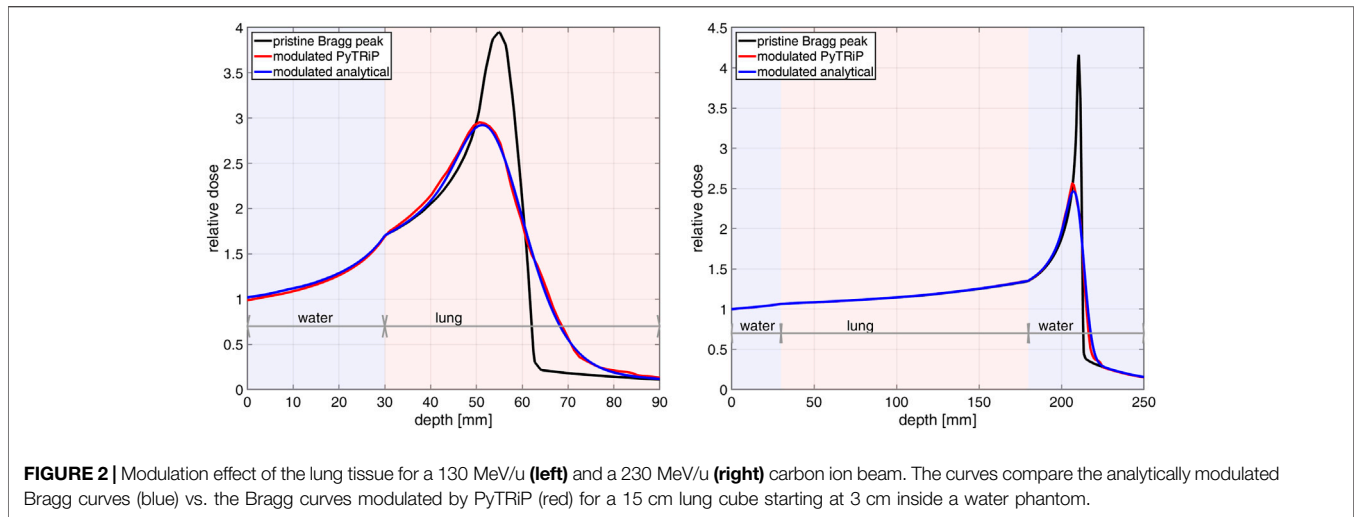
The comparisons of the Bragg curves can be seen in Figure 2. The agreement between the analytical curves and the curves from our PyTRiP routine is clearly seen.

### 2.2.3. Lung Voxel Selection Range

When selecting the  $VOI_{\text{lung}}$  voxels to be randomized, instead of using all voxels in the lung, we implemented a voxel selection by a user-defined density range  $\rho_{\text{range}}$ . By using all lung voxels, one would end up modulating a case-specific variable number of non-porous voxels such as massive vessels.

We adopted values of  $\rho_{\text{range}}$  from 0.1 to 0.5 g/cm<sup>3</sup> using experimental data from an inflatable pig lung set-up [4, 6, 8]





and visually analyzing the CT slices of our two patient cases and the density values of different structures observed within the lung. It is assumed that voxels within this range are lung voxels as well as any edge voxel that consists half of air and half of tissue. Both of these can lead to a modulation effect. In addition to this preselected range, we evaluated the effect on the patient plans when varying  $\rho_{\text{range}}$ .

### 2.3. Study of Spherical Planning Geometries

For a systematic analysis of the modulation effect as a function of the isocenter depth  $d_{ic}$  (placed at the PTV center) and the target size, plans for simulated spherical geometries were calculated for carbon ions. The spheres, composed of water, were placed within a cubic CT phantom, containing only voxels with a constant single Hounsfield unit value of  $-741$ , representing the lung environment [24].

First, a sphere of a constant 17 mm radius was placed at variable  $d_{ic}$  values of 40, 70, 100, 125, 150, 175, 200, 225, 250, and 260 mm. Second, spheres with variable radii, from 8 to 15 mm in steps of 1 mm, from 17 to 25 mm in steps of 2 mm, and of 28 mm, were placed at a constant  $d_{ic} = 100$  mm.

For the sphere planning study,  $n = 100$  and  $P_{mod} = 0.400$  mm were used and all lung voxels were taken into account for the modulation. All plans were single field plans with the beam parallel to the  $z$ -axis. A  $2 \times 2$  mm<sup>2</sup> lateral grid, a 3 mm depth step size and a lateral contour extension of  $0.7 \cdot FWHM_{iso}$  were used. All plans were optimized for the physical dose with the “ap”-algorithm. At  $d_{ic} = 40$  mm, a 4 mm bolus was required.

### 2.4. Patient Selection and Planning

Two lung cancer patient cases, henceforth called P1 and P2, with different PTV volumes  $V_{PTV}$  and locations were selected. They were originally treated with photons at the university hospital in Marburg. For P1 the PTV is deep-seated and located close to the spine, whereas the PTV for P2 is centrally located. For both cases, the tumors are not close to the thorax wall, as some distance in the lung is required for the degradation effect. The PTVs were sufficiently small as to not drastically decrease the lung

volume to be modulated. The isocenter slice of both patient geometries, P1 and P2, is given in Figure 3, showing for each patient case the PTV position and an exemplary dose distribution calculated on the non-modulated CTs.

Multiple plans for each of the two patients were created for protons as well as for carbon ions, focusing on the latter. For each nonmodulated case (planned on the nonmodulated CTs), planning parameters such as raster scan grid size, energy step size and optimization margins yielding the best PTV coverage with respect to dose conformity and target homogeneity were found by iterations. For the nonmodulated plans the planning objective was to deliver at least 95% of the prescribed dose to 98% of the PTV [25]. All plans were 1- or 2-field plans and optimized for physical (absorbed) dose. For the carbon ion cases, a 3 mm thick ripple filter was applied to broaden the BP, as is routine in the clinic [26].

Coplanar fields were used for the study. In order to have data with beams traversing different distances through the lung tissue  $s_{lung}$ , variable field angles were chosen. For the carbon ions, a horizontal field direction at  $0^\circ$  as well as  $-45^\circ$ ,  $+45^\circ$  and  $+90^\circ$  to horizontal were selected. For carbon ions dual-field plans with  $0^\circ$  and  $+45^\circ$  field angles and with  $0^\circ$  and  $+90^\circ$  field angles were

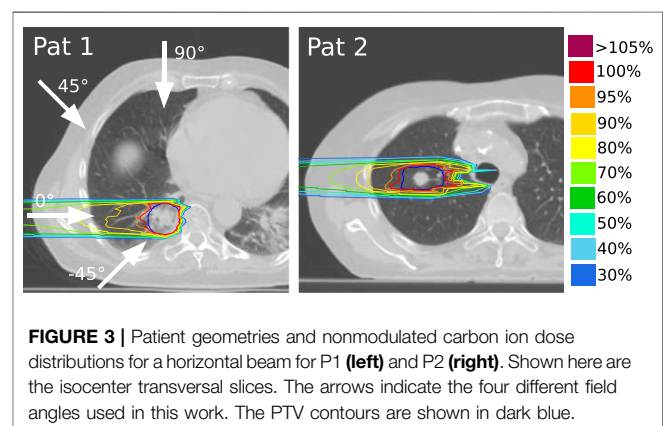


**TABLE 1** | PTV volumes  $V_{PTV}$  and estimated travel distances through the lung to the isocenter  $s_{lung}$  for both patient cases.

Patient	$V_{PTV}$ (cm <sup>3</sup> )	$s_{lung, 0^\circ}$ (mm)	$s_{lung, +45^\circ}$ (mm)	$s_{lung, -45^\circ}$ (mm)	$s_{lung, +90^\circ}$ (mm)
P1	41.9	74 ± 5	107 ± 5	62 ± 4	128 ± 5
P2	11.6	53 ± 4	58 ± 4	61 ± 4	65 ± 4

calculated as well. For protons  $0^\circ$ ,  $-45^\circ$ , and  $+45^\circ$  to horizontal was used for P1 and  $0^\circ$  for P2. The  $0^\circ$  and  $+45^\circ$  options match the fixed beamlines at the Marburger Ionenstrahl-Therapiezentrum and Shanghai Proton and Heavy Ion Center. Some of these field directions might not be clinically relevant, since sensitive structures and long distances through the lung are typically avoided, but were included here for investigative purposes. **Table 1** shows the  $s_{lung}$  for the investigated field angles and the  $V_{PTV}$  values. The  $s_{lung}$  values were estimated as the distance starting from the surface of the lung to the isocenter, placed in the middle of the PTV, along the central path of the beam. The  $V_{PTV}$  values were given by TRiP.

For protons, the “multiple scattering” algorithm was used for optimization and dose calculation, which considers the broadening of the beam as a function of patient depth [15]. For the carbon ion plans the much faster “all-points” algorithm, which is considering only all neighboring raster beam spots that may contribute to a given voxel [15], was used as this is normally sufficient for carbon ion plans [27]. Although comparisons between carbon ion plans with the two algorithms showed a slight difference in the plans (data not shown), the relative coverage difference between a modulated and nonmodulated dose distribution when comparing the algorithms was, even in the worst case, less than 0.5 percentual point (pp).

In addition to the main study, we calculated for the patient case P1 a range of carbon ion plans with lateral contour extensions from  $0.6 \cdot FWHM_{iso}$  to  $1.2 \cdot FWHM_{iso}$  in steps of 0.1, and for each of these with beam spot spacing of 2 and 3 mm and depth steps of 2 and 3 mm. A coplanar horizontal field was used for all plans. Dose distributions, calculated on the original CT, were compared to modulated doses with  $P_{mod} = 0.400$  mm and  $\rho_{range} = 0.1-0.5$  g/cm<sup>3</sup>. The goal was to estimate the influence of the planning parameters on the relative difference in PTV coverage between the nonmodulated and modulated dose distributions.

#### 2.4.1. Evaluation of the Parameters of the Lung Modulation Model

For the patient cases, the model parameters  $n$ ,  $d$ ,  $P_{mod}$  and  $\rho_{range}$  were evaluated.

The parameter  $n$  was evaluated for values of 24, 48, 72, 100, 120, 150, 200, and 400. For  $P_{mod}$ , we chose 0.300, 0.400, 0.500, and 0.600 mm, as our former works show that realistic values of  $P_{mod}$  lie below 0.600 mm. For the treatment planning cases with oblique fields for P1, plans with three different values of mean voxel length  $d$  were calculated: One following **Eq. 2** yielding  $d = 0.8439$  mm, one using the unchanged length of the voxel  $d = d_x = 0.9473$  mm, and the last value was obtained using the maximum

diagonal length through the voxel calculated with trigonometry as  $d = \sqrt{2} d_x = 1.339$  mm. The parameter  $\rho_{range}$  was evaluated by changing the maximum and minimum density value. We evaluated plans with  $\rho_{range}$  of 0.2–0.4, 0.2–0.5, 0.1–0.3, 0.1–0.4, 0.1–0.5, 0.0–0.5, 0.0–0.8, and 0.1–0.8 g/cm<sup>3</sup> and additionally ran calculations modulating all lung voxels.

After the parameter study was done, selected values of these parameters were then used throughout the paper:  $n = 100$ ,  $\rho_{range} = 0.1-0.5$  g/cm<sup>3</sup>,  $P_{mod} = 0.400$  mm and  $d$  corresponding to **Eq. 2**.

#### 2.4.2. Plan Evaluation

PTV coverage, dose homogeneity and planning conformity were used for dosimetric plan evaluations. In each patient case, the doses to lung, spinal cord, trachea and heart were compared between nonmodulated and modulated dose distributions.  $V_{95\%}$ , being the volume receiving at least 95% of the prescribed dose, was used for evaluating the PTV coverage. The homogeneity index (HI) and the conformity index (CI) were defined as:

$$HI = \frac{D_{2\%} - D_{98\%}}{D_{prescribed}} \quad (6)$$

$$CI = \frac{V_{95\%pi}}{V_{PTV}} \quad (7)$$

where  $V_{95\%pi}$  is the volume within the patient receiving 95% of the prescribed dose.

### 3. RESULTS

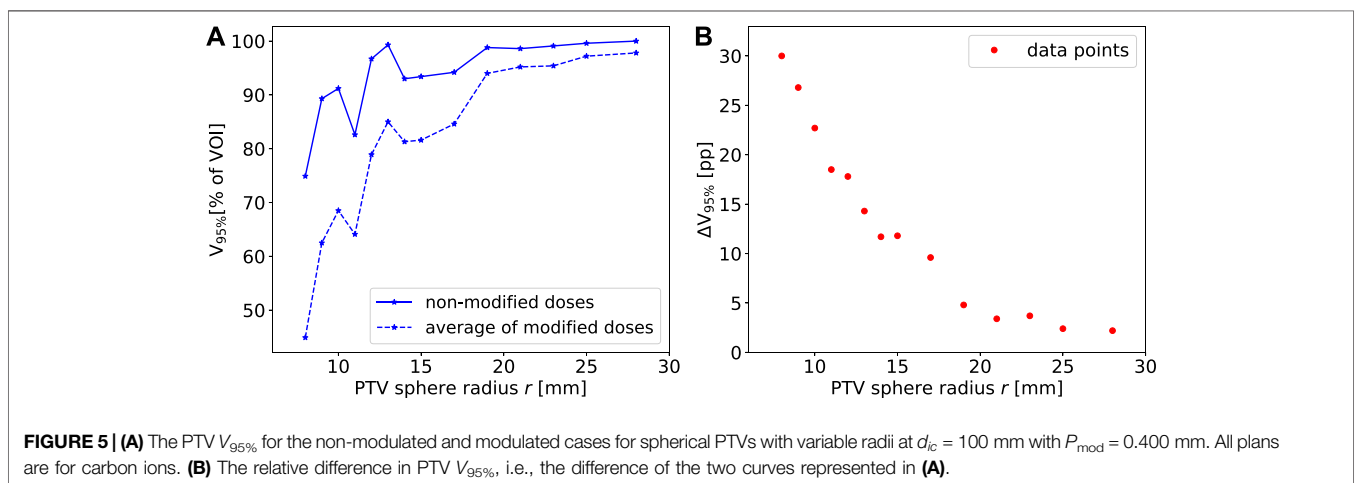
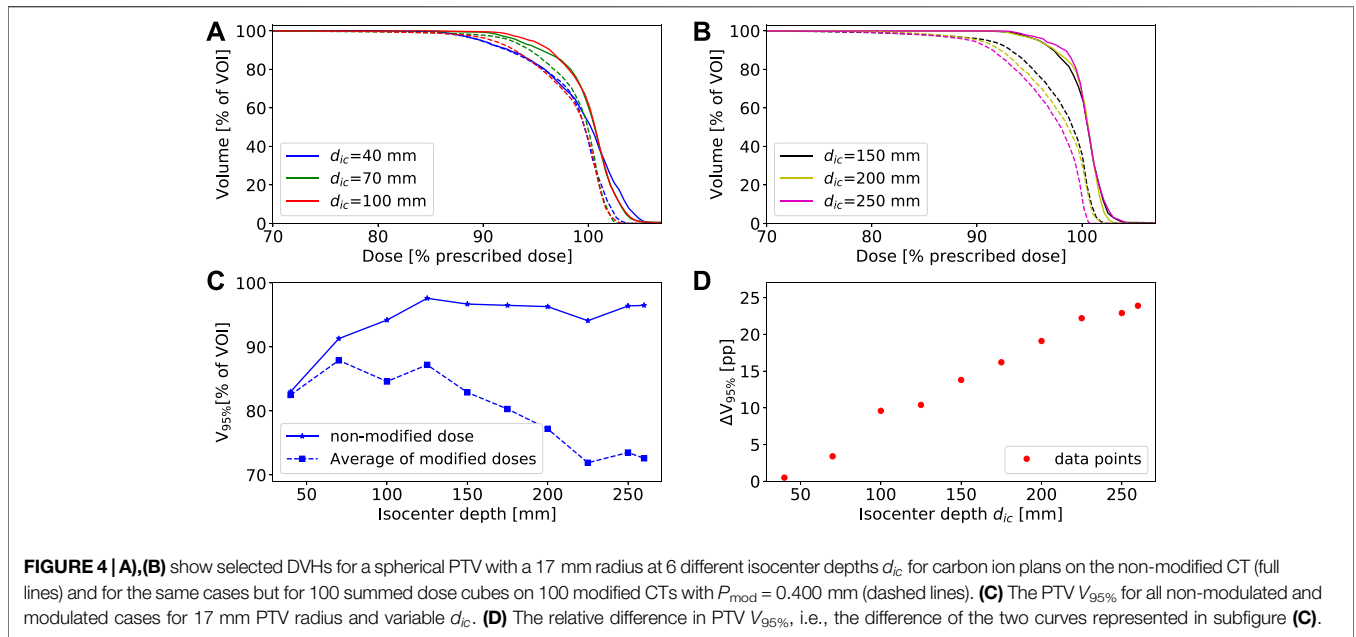
In general, the coverage and dose homogeneity of the PTVs were found to be worse for the modulated doses compared to the dose distributions calculated on the original CTs. This leads to a PTV dose overestimation by the TPS. The change in dose homogeneity was mainly due to a change in the minimum dose  $D_{98\%}$ . As expected, the relative difference between the modulated and nonmodulated dose distributions increases for larger values of  $P_{mod}$ .

From  $n = 72$  to 400 the dose distribution for the modified plans only changes with maximum 0.1 pp in  $V_{95\%}$  and  $D_{98\%}$ , while  $D_{2\%}$  remains constant. We adopted the value  $n = 100$  throughout the rest of the work.

#### 3.1. Spherical Geometries

**Figure 4** summarizes the results for modulated and nonmodulated dose distributions calculated for the spherical targets with 17 mm radius in a lung tissue CT cube. In **Figures 4A,B**, the DVHs for the nonmodulated and modulated dose distributions are shown for 6 different  $d_{ic}$  values. In **Figure 4C**,  $V_{95\%}$  as a function of  $d_{ic}$  is plotted for both the nonmodulated and modulated dose distributions and the differences between the corresponding pairs of values of the PTV coverage are shown in **Figure 4D**. **Figure 4D** shows a clear linear dependency of the relative difference in coverage as a function of  $d_{ic}$ .

In **Figure 5A**, the  $V_{95\%}$  values for plans with  $d_{ic} = 100$  mm and variable PTV radii are shown. The relative difference in



$V_{95\%}$  between the nonmodulated and modulated dose distributions is given in **Figure 5B**. In general the larger the PTV volume the better the coverage for both the nonmodulated and modulated dose distributions with an approximated exponential decrease of the relative coverage difference with PTV radius.

In both cases of **Figures 4C, 5A**, some outliers can be seen in the individual  $V_{95\%}$ -curves. Importantly, they occur for both the nonmodulated and modulated case, leaving their relative difference consistent. This is to be expected as the “modulated plans” are dose recomputations of the nonmodulated ones. Similar curve shapes were seen when using other coverage indices, as for example  $V_{90\%}$ ,  $V_{80\%}$  or the mean dose (data not shown). One deviation from the smooth tendency that can be easily explained is the very superficial case at  $d_{ic} = 40$  mm. Here,

there is very little lung tissue in front of the PTV, resulting in a marginal difference between the nonmodulated and modulated dose distributions. Additionally, due to the low beam energies required at such low depth, a 4 mm bolus was applied, which might lead to an inferior coverage independently of the lung modulation effect.

### 3.2. Patient Plans

Dosimetric indexes  $V_{95\%}$ ,  $D_{98\%}$ ,  $D_{2\%}$  and dose homogeneity HI of the carbon ion patient plans are presented in **Table 2** (for P1) and **Table 3** (for P2) for the nonmodulated cases and for the recalculated modulated dose distributions. The planning cases for P2 for  $\pm 45^\circ$  field angles have been omitted due to not fulfilling the planning objectives. In **Table 2**, dosimetric indices are additionally given for the three different values of

**TABLE 2 |** Dosimetric indices for carbon ion treatment plans for P1 with  $\rho_{range}$  of 0.1–0.5 g/cm<sup>3</sup> and different planning parameters.

Field angles	$P_{mod}$ (mm)	$V_{95\%}$ (%)	$D_{98\%}$ (%)	$D_{2\%}$ (%)	HI
0°	Non-mod	98.7	96.9	102.8	0.059
0°	0.300	95.6	90.7	101.7	0.110
0°	0.400	94.2	88.9	101.6	0.127
0°	0.500	92.9	86.9	101.6	0.147
0°	0.600	91.1	84.7	101.5	0.168
+45°	Non-mod	99.0	96.9	102.9	0.060
+45°	0.300	95.0	91.3	101.8	0.105
+45°	0.400	93.2	89.1	101.7	0.126
+45°	0.500	91.1	86.9	101.7	0.148
+45°	0.600	88.5	84.0	101.7	0.177
+45°, $d = d_x$	0.300	95.6	91.8	101.8	0.100
+45°, $d = d_x$	0.400	94.0	90.3	101.8	0.115
+45°, $d = d_x$	0.500	92.4	88.8	101.7	0.129
+45°, $d = d_x$	0.600	90.6	86.5	101.7	0.152
+45°, $d = \sqrt{2} d_x$	0.300	96.1	92.3	101.9	0.096
+45°, $d = \sqrt{2} d_x$	0.400	94.7	90.8	101.9	0.111
+45°, $d = \sqrt{2} d_x$	0.500	93.3	89.5	101.8	0.123
+45°, $d = \sqrt{2} d_x$	0.600	91.7	87.6	101.8	0.142
-45°	Non-mod	99.4	98.4	102.0	0.036
-45°	0.300	98.6	96.3	101.6	0.053
-45°	0.400	98.3	95.6	101.6	0.060
-45°	0.500	97.7	94.7	101.5	0.068
-45°	0.600	97.4	94.1	101.5	0.074
-45°, $d = d_x$	0.300	98.7	96.6	101.6	0.050
-45°, $d = d_x$	0.400	98.4	95.8	101.6	0.058
-45°, $d = d_x$	0.500	98.1	95.2	101.6	0.064
-45°, $d = d_x$	0.600	97.7	94.7	101.6	0.069
-45°, $d = \sqrt{2} d_x$	0.300	98.8	96.7	101.6	0.049
-45°, $d = \sqrt{2} d_x$	0.400	98.5	96.0	101.6	0.056
-45°, $d = \sqrt{2} d_x$	0.500	98.3	95.6	101.6	0.060
-45°, $d = \sqrt{2} d_x$	0.600	97.8	94.8	101.6	0.068
+90°	Non-mod	99.1	96.8	102.4	0.056
+90°	0.300	98.1	95.6	102.1	0.065
+90°	0.400	97.6	94.7	102.1	0.074
+90°	0.500	97.0	93.8	102.1	0.083
+90°	0.600	96.2	93.0	102.0	0.090
0° and +45°	Non-mod	99.3	97.0	101.6	0.046
0° and +45°	0.300	98.2	95.3	101.4	0.061
0° and +45°	0.400	97.7	94.6	101.3	0.067
0° and +45°	0.500	97.2	94.1	101.3	0.072
0° and +45°	0.600	96.3	92.8	101.3	0.085
0° and +90°	Non-mod	99.4	97.5	102.2	0.047
0° and +90°	0.300	98.4	96.0	101.7	0.057
0° and +90°	0.400	97.9	95.2	101.7	0.065
0° and +90°	0.500	97.4	94.4	101.7	0.073
0° and +90°	0.600	96.8	93.7	101.6	0.079

Were  $d$  is not stated, it was calculated following Eq. 2. For the cases of the modulated dose distributions,  $n = 100$ .

$d$  used for the oblique beam cases. Dosimetric indexes for the proton patient plans are given in Table 4 for both patient cases.

DVHs for PTV, trachea and lung in the nonmodulated and modulated dose distributions in selected one-beam plans for P1 (horizontal and oblique beams) and P2 (horizontal beam) are shown for carbon ions and protons in Figures 6, 7, respectively. No difference was found in the DVHs with and without lung modulation for the organs not displayed in these graphs. Zoomed plots for the DVHs of the PTV help to see the relative differences between nonmodulated and modulated dose distributions.

**TABLE 3 |** Dosimetric indices for carbon ion treatment plans for P2 with  $\rho_{range}$  of 0.1–0.5 g/cm<sup>3</sup> and different planning parameters.

Field angles	$P_{mod}$ (mm)	$V_{95\%}$ (%)	$D_{98\%}$ (%)	$D_{2\%}$ (%)	HI
0°	Non-mod	98.4	95.6	103.1	0.075
0°	0.300	97.5	94.4	101.6	0.072
0°	0.400	96.8	93.6	101.4	0.077
0°	0.500	96.2	92.9	101.2	0.083
0°	0.600	95.0	91.4	101.1	0.097
+90°	Non-mod	97.4	93.2	103.0	0.098
+90°	0.300	96.2	91.5	101.3	0.098
+90°	0.400	95.4	90.4	101.1	0.107
+90°	0.500	93.4	86.6	101.1	0.145
+90°	0.600	91.2	85.0	101.0	0.161
0° and +45°	Non-mod	99.3	97.0	102.5	0.055
0° and +45°	0.300	97.1	93.4	100.9	0.075
0° and +45°	0.400	95.3	92.1	100.8	0.087
0° and +45°	0.500	93.0	89.8	100.6	0.108
0° and +45°	0.600	90.9	88.8	100.6	0.118

The value of  $d$  was calculated following Eq. 2. For the cases of the modulated dose distributions,  $n = 100$ .

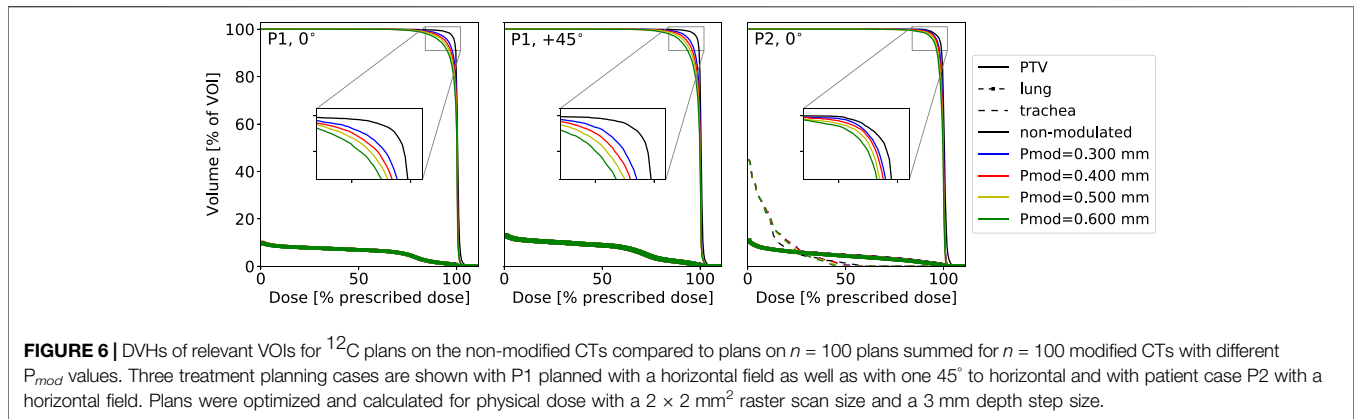
As can be seen comparing Tables 2–4 and by comparing Figures 6, 7, the relative differences between nonmodulated and modulated dose distributions are larger for carbon ions than for protons, which can be attributed to the generally sharper carbon ion BPs. Actually, for all cases of the modulated proton plans for P1, the drop in  $V_{95\%}$  never compromised the planning objective of giving at least 95% prescribed dose to 98% of the PTV volume. Our conclusion is that the lung modulation effect is not very severe for proton treatment planning. This is in agreement with other findings [10, 11]. We focus on the carbon ions plans for further analysis due to the larger modulation effect observed for this particle type relative to protons.

**TABLE 4 |** Dosimetric indices for proton treatment plans for P1 and P2 with  $\rho_{range}$  of 0.1–0.5 g/cm<sup>3</sup> and different planning parameters for each for the two patients.

Planning case	$P_{mod}$ (mm)	$V_{95\%}$ (%)	$D_{98\%}$ (%)	$D_{2\%}$ (%)	HI
P1, 0°	Non-mod	99.6	99.0	101.5	0.025
P1, 0°	0.300	99.3	98.7	101.1	0.032
P1, 0°	0.400	99.0	97.5	101.1	0.036
P1, 0°	0.500	98.8	96.8	101.0	0.041
P1, 0°	0.600	98.5	96.1	101.0	0.049
P1, +45°	Non-mod	99.5	97.4	102.6	0.052
P1, +45°	0.300	99.0	96.8	101.8	0.050
P1, +45°	0.400	98.7	96.2	101.7	0.055
P1, +45°	0.500	98.3	95.7	101.7	0.059
P1, +45°	0.600	98.0	95.0	101.7	0.067
P1, -45°	Non-mod	99.5	97.8	102.4	0.046
P1, -45°	0.300	99.4	97.7	102.1	0.044
P1, -45°	0.400	99.2	97.4	102.1	0.047
P1, -45°	0.500	99.1	97.2	102.1	0.049
P1, -45°	0.600	99.1	97.1	102.1	0.050
P2, 0°	Non-mod	99.3	97.6	102.3	0.047
P2, 0°	0.300	98.1	95.2	101.7	0.065
P2, 0°	0.400	97.7	94.3	101.7	0.073
P2, 0°	0.500	97.0	93.0	101.5	0.086

For the modulated doses,  $n = 100$ .





Of all the displayed DVHs, only those corresponding to the trachea for the case P2 exhibit a slightly changed maximum dose when considering the lung modulation effect ( $D_{2\%}$  changes from 45.5% of the prescribed dose for the non-modulated plan to 38.9% for the case of  $P_{\text{mod}} = 0.600 \text{ mm}$ ). In the low dose region, the DVH for the trachea is slightly larger for the modified doses compared to the nonmodulated one. For example  $V_{20\%} = 7.3\%$  of the prescribed dose for the nonmodulated dose compared to 10.4% of the prescribed dose for the dose distribution calculated with  $P_{\text{mod}} = 0.600 \text{ mm}$ . None of these findings bear however a clinical relevance.

The dose to the lung displays minimal changes between modulated and nonmodulated dose distributions. Due to the generally smaller beam spot sizes of carbon ion beams, the ipsilateral lung could be better spared using carbon ions with approximately half the integral dose given to the lung compared to the proton plans. As an example, for P1, the  $V_{5\%}$  with a horizontal proton beam is 18.8% of the prescription dose compared to 8.9% delivered with carbon ions.

Due to the tumor location of the selected patients, far from critical organs (the spinal cord for example), we will focus on assessment of the changes in target coverage as presented in Tables 2–4.

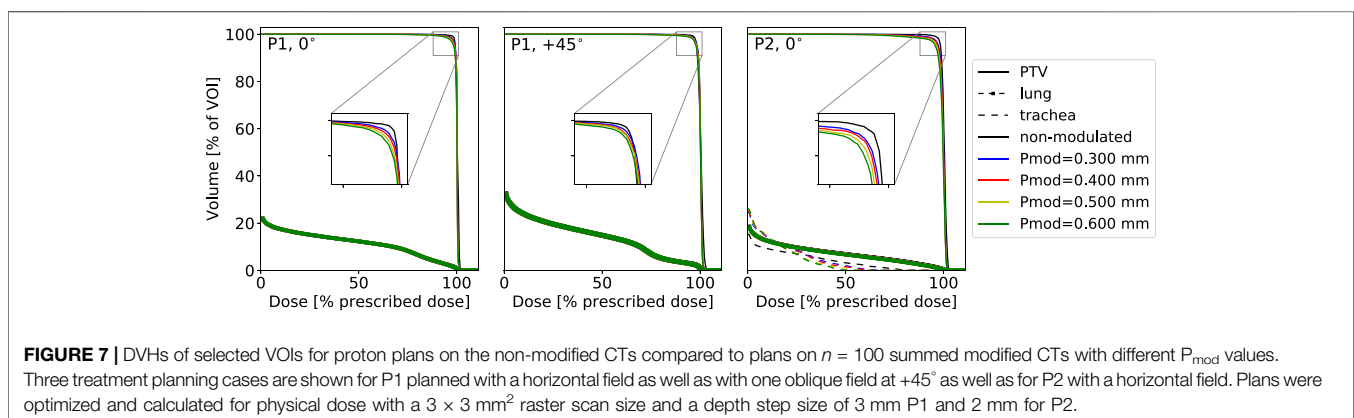
In Figure 8 is shown the relative difference between the  $V_{95\%}$  of the nonmodulated doses and the modulated doses calculated for the values of  $P_{\text{mod}} = 0.300 \text{ mm}$  (blue plots) and  $P_{\text{mod}} =$

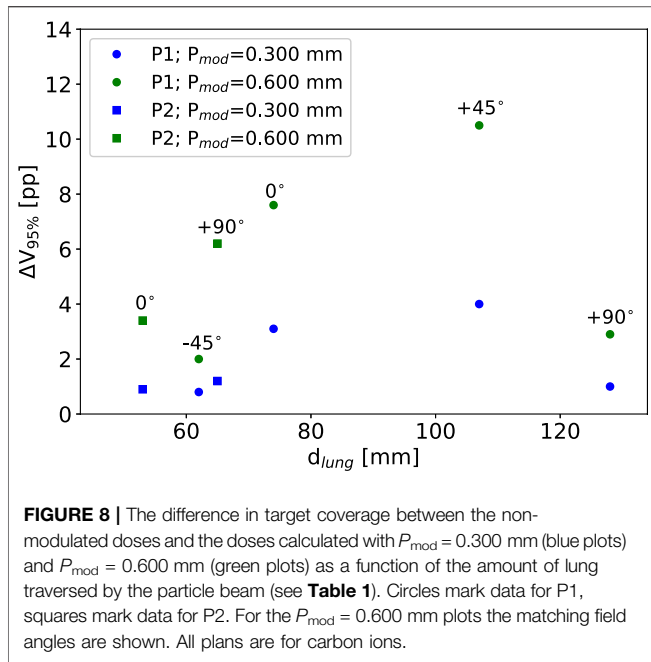
0.600 mm (green plots) as a function of the distance traversed through the lung  $s_{\text{lung}}$ . The general trend of the sphere study, that a larger relative difference is seen for smaller PTV sizes, is present. However, that the relative difference is larger for a larger value of  $s_{\text{lung}}$  is only partially confirmed. For P1, when comparing the single field plans at  $0^\circ$  and  $+45^\circ$ , the relative differences between the nonmodulated and modulated dose distributions are larger for the  $+45^\circ$  case. This is expected since at this angle the beam traverses a larger amount of lung tissue. However, the beam at  $0^\circ$  yields a larger relative difference than for  $-45^\circ$  by a large margin, even for the lowest  $P_{\text{mod}}$  value, although  $s_{\text{lung}}$  is slightly lower for the  $-45^\circ$  setup. For the largest  $s_{\text{lung}}$  value at  $+90^\circ$ , a much smaller relative difference between nonmodulated and modulated doses are observed than for the  $0^\circ$  and  $-45^\circ$  angles.

In the clinic, single field plans would rarely be used. Therefore, we also included selected few dual-field plans in the study. The dual-field plans are providing better and more conform target coverage, also for the nonmodulated doses and it can be seen that the drop in target coverage caused by the beam-modulation effect is slightly smaller for the dual-field plans relative to the nonmodulated ones.

### 3.2.1. The Effect of the Voxel Length $d$

As expected, and as can additionally be seen in Table 2, the relative difference between the plans with different values of  $d$  are significantly larger for the  $+45^\circ$  cases where the particles traverse





roughly twice the amount of lung tissue compared to the  $-45^\circ$  cases. Also, it can be seen that the larger the value of  $P_{mod}$ , the more critical a variation in  $d$  becomes. However, even for  $+45^\circ$  the largest decrease in  $V_{95\%}$  seen between  $d = 0.8439$  mm and  $d = 1.339$  mm is 2.9 pp. For  $-45^\circ$ , the largest decrease is only 0.4 pp.

### 3.2.2. Selecting Modulation Lung Voxels

Dosimetric indexes for plans with  $P_{mod} = 0.400$  mm and variable  $\rho_{range}$  values are listed in **Table 5** for carbon ion plans and **Table 6**

**TABLE 5 |** Dosimetric indices for carbon ion plans for patients P1 and P2 and  $P_{mod} = 0.400$  mm for variable values of  $\rho_{range}$ .

Planning case	$\rho_{range}$ (g/cm <sup>3</sup> )	$V_{95\%}$ (%)	$D_{98\%}$ (%)	$D_{2\%}$ (%)	HI
P1	Non-mod	98.7	96.9	102.8	0.059
P1	0.2–0.4	95.9	91.6	101.6	0.100
P1	0.2–0.5	94.9	89.8	101.7	0.119
P1	0.1–0.3	96.5	92.2	101.8	0.095
P1	0.1–0.4	95.3	90.0	101.7	0.117
P1	0.1–0.5	94.2	88.9	101.6	0.127
P1	0.0–0.5	94.1	88.7	101.7	0.130
P1	0.1–0.8	92.2	86.3	101.6	0.153
P1	0.0–0.8	92.1	86.0	101.5	0.155
P1	All voxels	91.7	85.8	101.6	0.158
P2	Non-mod	98.4	95.6	103.1	0.075
P2	0.2–0.4	97.8	94.7	102.0	0.073
P2	0.2–0.5	97.7	94.6	102.1	0.075
P2	0.1–0.3	97.6	94.7	101.6	0.069
P2	0.1–0.4	97.1	94.1	101.5	0.074
P2	0.1–0.5	96.8	93.6	101.4	0.077
P2	0.0–0.5	97.1	93.9	101.4	0.075
P2	0.1–0.8	96.4	93.2	101.3	0.081
P2	0.0–0.8	96.4	92.9	101.3	0.084
P2	All voxels	96.0	92.5	101.2	0.087

All plans are calculated with horizontal fields, e.g., with the  $+0^\circ$  option with planning parameters given in the material and methods section.

for proton plans. Values for the nonmodulated cases are given for comparison.

The same trends for  $V_{95\%}$  and HI as for  $\rho_{range} = 0.1–0.5$  g/cm<sup>3</sup> are seen. For protons, the dependency of the  $\rho_{range}$  parameter on the plans is generally much lower when compared to carbon ions, as the relative differences between modulated and nonmodulated dose distributions are generally lower for protons. In the case of the largest variation for the protons plans, there is a decrease in  $V_{95\%}$  of 1.4 pp when using the narrowest  $\rho_{range}$  of 0.2–0.4 g/cm<sup>3</sup> compared to using all the voxels in the ipsilateral lung. There HI has an increase of approximately 43%. In comparison, for the carbon ions, the extreme case of P1 shows a decrease in  $V_{95\%}$  of 4.2 pp when comparing  $\rho_{range} = 0.2–0.4$  g/cm<sup>3</sup> with using all the voxels and an 58% HI increase. The less severe case of P2 shows for the same comparison a coverage drop of only 1.8 pp and a small HI increase of 16%.

Both of the extreme cases,  $\rho_{range} = 0.2–0.4$  g/cm<sup>3</sup> or no fixed  $\rho_{range}$ , are unrealistic choices. For P2, the  $V_{95\%}$  values of the experimentally estimated  $\rho_{range} = 0.1–0.5$  g/cm<sup>3</sup> lie in between the values of these two extremes for both protons and carbon ions. For protons, this is also the case for P1. For carbon ions for P1, the difference in  $V_{95\%}$  from  $\rho_{range} = 0.2–0.4$  g/cm<sup>3</sup> to  $\rho_{range} = 0.1–0.5$  g/cm<sup>3</sup> is 1.7 pp, while for  $\rho_{range} = 0.1–0.5$  g/cm<sup>3</sup> compared to the case with no  $\rho_{range}$  limit is 2.5 pp.

### 3.2.3. Effect of Changes on the Planning Parameter Settings

**Figure 9** shows a boxplot with outliers for coplanar horizontal field plans for P1 with variable planning parameters (see the materials and methods section). Nonmodulated and modulated doses, calculated with  $P_{mod} = 0.400$  mm, are shown separately. All plans that in the nonmodulated cases had  $V_{95\%}$  below 98.0% or a

**TABLE 6 |** Dosimetric indices for proton plans for patients P1 and P2 and  $P_{mod} = 0.400$  mm for variable values of  $\rho_{range}$ .

Planning case	$\rho_{range}$ (g/cm <sup>3</sup> )	$V_{95\%}$ (%)	$D_{98\%}$ (%)	$D_{2\%}$ (%)	HI
P1	Non-mod	99.6	99.0	101.3	0.023
P1	0.2–0.4	99.2	97.8	101.0	0.032
P1	0.2–0.5	99.2	97.7	101.1	0.034
P1	0.1–0.4	99.2	97.7	101.0	0.033
P1	0.1–0.3	99.4	98.3	101.0	0.027
P1	0.1–0.5	99.1	97.5	101.1	0.036
P1	0.0–0.5	99.0	97.4	101.1	0.037
P1	0.1–0.8	98.8	96.8	101.1	0.043
P1	0.0–0.8	98.8	96.7	101.1	0.044
P1	All voxels	98.7	96.5	101.2	0.047
P2	Non-mod	99.3	97.6	102.3	0.047
P2	0.2–0.4	98.5	96.3	101.7	0.054
P2	0.2–0.5	98.4	96.0	101.6	0.056
P2	0.1–0.3	98.9	94.8	101.5	0.067
P2	0.1–0.4	98.0	95.0	101.6	0.066
P2	0.1–0.5	97.8	94.4	101.7	0.072
P2	0.0–0.5	97.8	94.4	101.6	0.071
P2	0.1–0.8	97.3	93.4	101.6	0.082
P2	0.0–0.8	97.3	93.7	101.6	0.080
P2	All voxels	97.1	93.2	101.5	0.083

All plans are calculated with horizontal fields, e.g. with the  $+0^\circ$  option with planning parameters given in the material and methods section.

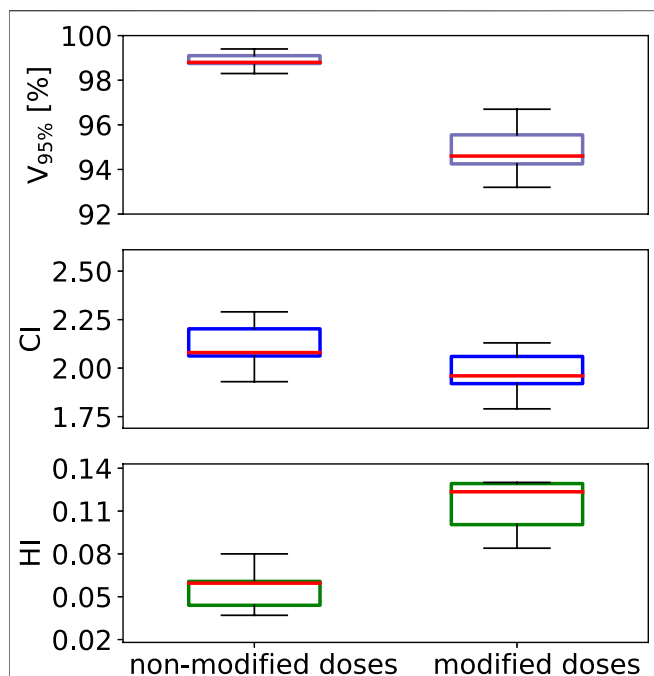


**FIGURE 9** | A standard boxplot (median, 1. and 3. quartiles and whiskers including the outliers) for  $V_{95\%}$ , HI and CI data sets obtained for patient case P1 using a horizontal beam for non-modulated as well as modulated dose distributions for carbon ions. A set of variable planning parameters was used as given in the materials and method section.

CI above 2.5 were omitted from this study, as they did not fulfill the planning objectives.

It is seen how  $V_{95\%}$ , for the modulated dose distributions, varies more from a change in planning parameters. We observed that the better the nonmodulated plan was, in terms of PTV coverage and dose homogeneity, the smaller the relative difference between the nonmodulated and the modulated dose distribution.

For a small number of plans with specific parameter settings, the dose distribution was even improved by the lung modulation, in terms of PTV coverage and homogeneity. It was seen that, in some cases, it is possible to first calculate an inferior plan for the nonmodulated case, which due to the broader and slightly displaced BPs caused by the lung-modulation effect can result in a plan fulfilling the planning objectives for the modulated case. As an example, we show in **Figure 10** DVHs for a plan calculated on patient case P2, for a non-modified case (solid lines) compared to the sum of doses calculated on 100 modified CTs (dashed lines). A horizontal field was used, with beam spot spacing of 3 mm, energy step 3 mm, and lateral contour extension  $1.2 \cdot \text{FWHM}_{\text{iso}}$  with values of  $P_{\text{mod}} = 0.400$  mm and  $\rho_{\text{range}} = 0.1\text{--}0.5$  g/cm<sup>3</sup> for the calculation of the modulation effect.  $V_{95\%} = 97.7\%$  and  $\text{HI} = 0.102$  were found for the nonmodulated doses and  $V_{95\%} = 97.0\%$  and  $\text{HI} = 0.061$  were found for modulated doses, respectively. Although the values of the PTV coverage were similar for these two cases and slightly lower still for the modulated case, the HI value was reduced by one third after the modulation, as the much steeper fall-off for that DVH curve in **Figure 10** also illustrates.

## 4. DISCUSSION

The beam-modulation effect caused by the porous material of the lung results in a lower PTV coverage and dose homogeneity. This effect is clearly more pronounced for carbon ions than for protons, as the sharper the initial BP the stronger the modulation effect. The modulation effect is generally negligible in proton treatments, as compared to the other dose delivery and treatment uncertainties related to protons, which confirms the work of Baumann et al. [10]. Among such uncertainties are particle range uncertainties, patient setup errors, inter-fractional anatomy changes (e.g., weight loss, tumor shrinkage, etc.) and intra-fractional tumor motion. Additionally, TPS algorithms often have problems handling the air cavities and sharp density gradients present in the lung.

Using spherical geometries, we show that when 1) increasing the distance the beam travels through the lung tissue and/or when 2) reducing the PTV size, the effect of the beam-modulation increases. Both tendencies have been shown previously only for protons [9]. The latter effect fits the general knowledge that a good PTV coverage is more difficult to obtain for smaller PTVs when using broader BPs. For the non-modulated plans, the PTV coverage increases with an increasing depth, while for the modulated cases, the larger the depth of the target in the lung the larger the beam-modulation effect. This altogether yields the increasing relative difference with depth between the non-modulated and modulated dose distributions.

These trends were only partially confirmed for the patient cases. The systematic study on spherical target geometries represents a simplified scenario, while for patient cases there are many degrees of freedom and many further parameters in

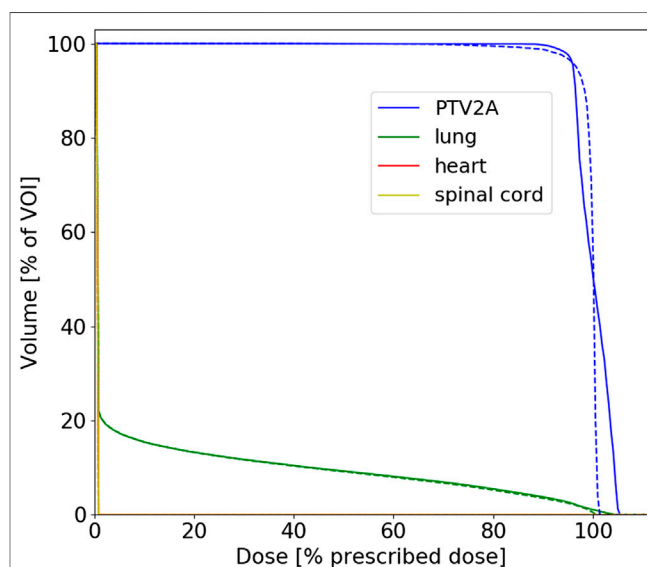


**FIGURE 10** | DVHs for proton plans calculated on patient case P2 for non-modified (solid lines) vs. sum of 100 modified CTs (dashed lines). The corresponding planning parameters and dosimetric indexes are given in the text.

consideration, such as case-dependent planning parameters and much more complex patient geometries. The angle from which the beam comes might lead to a large change in the relative difference between modulated and nonmodulated dose distributions. Our conclusions are based on our limited number of planning cases, but in this work, a wider general test of the lung modulation model as well as the systematic study with spheres were prioritized.

The largest uncertainties in our model (and as an extension in any similar routine dealing with the lung modulation) lie in the parameters  $P_{\text{mod}}$  and  $\rho_{\text{range}}$ . As  $P_{\text{mod}}$  has been investigated in other works, we focused on  $\rho_{\text{range}}$ , which has not been studied before. A too large  $\rho_{\text{range}}$  would mean that non-porous biological lung structures, such as massive vessels, are falsely taken into account as porous voxels and the calculated modulation effect would be slightly larger than the actual modulation. On the other hand, by choosing a too small  $\rho_{\text{range}}$  the modulation effect of the lung would be underestimated, which in particular for heavier ions can be important (as the effect is more pronounced for heavier ions as indicated in this work). We found that the upper limit might be more critical than the lower limit, since a too low upper limit would filter out too much porous lung material from the calculation. As long as the lower limit is kept within a reasonable value, which can easily be determined from CT voxel histograms, this value only marginally influences the modulation results. One should do at least a manual filtering of voxels containing visible big vessels and/or similar biological structures, which should not be modified.

Another, less important, parameter in the model is the voxel length  $d$ . For beam angles running parallel to the CT axis  $d$  is trivially the voxel length in that direction whereas, for any other angles, it must be calculated. The effect on the lung modulation of the value of  $d$  was found to be not so dramatic and only important when the distance through the lung traveled by the particles is large. We recommend using the tested formula, given in this work as Eq. 2.

The specifically chosen example shown in Figure 10 might indicate that, in some rare planning cases, an inferior dose coverage of the PTV can actually be improved by the lung modulation effect, although, in the large majority of cases, not taking the lung modulation effect into consideration in treatment planning is a net disadvantage for the patients.

The mathematical model described in this work could, in theory, be built into other TPSs too. We note, although, that the “future” of implementing the lung modulation into a TPS lies within MC codes when these will be coupled to treatment planning in a more general way. MC codes allow for on-the-fly modulation of the voxels during the actual treatment planning process and not by recomputing the dose on many different modulated CTs, followed by summing up the dose distribution to estimate the modulation effect. However, even with MC available, for the case that a deterministic TPS mode would still be opted for—for instance to calculate biologically effective dose with the Linear Effect Model (LEM) [14, 28]—the concept presented in this work is an appropriate option for recalculation of treatment plans and for assessment of the lung modulation effect. For carbon ion therapy, the authors

estimate that TPS with deterministic pencil algorithms are assumed to remain still in clinical use in the next years. Additionally, deterministic TPS programs, like TRiP98 and matRad [11], will play an important role for educational purposes.

## 5. CONCLUSION

With existing standard tools, it is possible in a transparent and reproducible way, to implement and calculate the beam-modulation effect of the lung in a known TPS for particles. Our evaluation of two selected lung cancer patients is in line with previous results. For protons, the lung modulation effect is found to be negligible compared to other dose delivery uncertainties related to particle therapy treatments of the lung. For carbon ions, the effect is significantly more pronounced and cannot be ignored. The decrease in both PTV coverage and dose homogeneity, caused by the modulation effect, could lead to underdosage within the PTV and to overdosage in the healthy normal tissue surrounding the PTV. Planning parameters and beam angles also have an impact on the relative difference between nonmodulated dose distributions and those taking the beam-modulation effect into account, caused by the porous nature of lung tissue.

## DATA AVAILABILITY STATEMENT

The original contributions presented in the study are included in the article, further inquiries can be directed to the corresponding author.

## ETHICS STATEMENT

Ethical review and approval was not required for the study on human participants in accordance with the local legislation and institutional requirements. Written informed consent from the participants was not required to participate in this study in accordance with the national legislation and the institutional requirements.

## AUTHOR CONTRIBUTIONS

UW devised the project, the main conceptual ideas and project outline. TR, AS, KZ, and UW further developed the project with AS and KZ supervising the work and providing financial support. TR, LG, and NB developed the software tools for the manuscript, based on a mathematical model developed by UW. TR performed the computations, the data gathering and the data analysis. TR and AS created the images and graphs. KB, VF, and RE provided the patient data. TR wrote the manuscript with input from all authors.

## FUNDING

The authors TR and AS acknowledge the financial support of the German fund for research “Deutsche Forschungsgemeinschaft” (DFG), case number SA 3085/1-1, Granted to AS. The study was also performed in the frame of FAIR Phase-0 supported by the GSI Helmholtzzentrum für Schwerionenforschung in Darmstadt (Germany).

## REFERENCES

- Haberer T, Becher W, Schardt D, Kraft G. Magnetic scanning system for heavy ion therapy. *Nucl Instrum Methods Phys Res Sect A Accel Spectrom Detect Assoc Equip* (1993) 330:296. doi:10.1016/0168-9002(93)91335-k
- Lomax AJ, Bortfeld T, Goitein G, Debus J, Dykstra C, Tercier P-A, et al. Treatment planning inter-comparison of proton and intensity modulated photon radiotherapy. *Radiother Oncol* (1999) 51:257–71. doi:10.1016/s0167-8140(99)00036-5
- Coucke GO, Titt U, Mirkovic D, Mohan R. Density heterogeneities and the influence of multiple Coulomb and nuclear scatterings on the Bragg peak distal edge of proton therapy beams. *Phys Med Biol* (2008) 53:4605–19. doi:10.1088/0031-9155/53/17/010
- Ringbæk TP, Simeonov Y, Witt M, Cabillic-Engenhart R, Kraft G, Zink K, et al. Modulation power of porous materials and usage as ripple filter in particle therapy. *Phys Med Biol* (2017) 62:2892–909. doi:10.1088/1361-6560/aa5c28
- Titt U, Sell M, Unkelbach J, Bangert M, Mirkovic D, Oelfke U, et al. Degradation of proton depth dose distributions attributable to microstructures in lung-equivalent material. *Med Phys* (2015) 42:6425–32. doi:10.1118/1.4932625
- Mohan K-S, Witt M, Weber U, Engenhart-Cabillic R, Zink K. An efficient method to predict and include Bragg curve degradation due to lung-equivalent materials in Monte Carlo codes by applying a density modulation. *Phys Med Biol* (2017) 62:3997–4016. doi:10.1088/1361-6560/aa641f
- Espana M, Paganetti H. Uncertainties in planned dose due to the limited voxel size of the planning ct when treating lung tumors with proton therapy. *Phys Med Biol* (2011) 56:3472–56. doi:10.1088/0031-9155/56/13/007
- Witt M, Weber U, Simeonov Y, Zink K. SU-E-T-671: range-modulation effects of carbon ion beams in lung tissue. *Med Phys* (2015) 42:3491. doi:10.1118/1.4925034
- Flatten V, Baumann K, Weber U, Engenhart-Cabillic R, Zink K. Quantification of the dependencies of the Bragg peak degradation due to lung tissue in proton therapy on a ct-based lung tumor phantom. *Phys Med Biol* (2019) 64:155005. doi:10.1088/1361-6560/ab2611
- Baumann K, Flatten V, Weber U, Lautenschläger S, Eberle F, Zink K, et al. Effects of the Bragg peak degradation due to lung tissue in proton therapy of lung cancer patients. *Radiat Oncol* (2019) 14:155005. doi:10.1186/s13014-019-1375-0
- Winter J, Ellerbrock M, Jäkel O, Greulich S, Bangert M. Analytical modeling of depth-dose degradation in heterogeneous lung tissue for intensity-modulated proton therapy planning. *Phys Imaging Radiat Oncol* (2020) 14:32–8. doi:10.1016/j.phro.2020.05.001
- Wieser H-P, Cisternas E, Wahl N, Ulrich S, Stadler A, Mescher H, et al. Development of the open-source dose calculation and optimization toolkit matrad. *Med Phys* (2017) 44:2556–68. doi:10.1002/mp.12251
- Müller M, Jäkel O, Haberer T, Kraft G, Schardt D, Weber U. Treatment planning for heavy-ion radiotherapy: physical beam model and dose optimization. *Phys Med Biol* (2000) 45:3299–317. doi:10.1088/0031-9155/45/11/313
- Krämer M, Scholz M. Treatment planning for heavy-ion radiotherapy: calculation and optimization of biologically effective dose. *Phys Med Biol* (2000) 45:3319–30. doi:10.1088/0031-9155/45/11/314

## ACKNOWLEDGMENTS

The authors acknowledge the access to TRiP98, provided by M. Krämer and the GSI, and the cluster time at the PLGRID infrastructure in Krakow under Grant Number ccbmc7. The authors Ringbæk and Santiago acknowledge the support of M. Stuschke and S. Qamhiyeh from the Radiotherapy Department at Essen University Hospital. We thank Michelle Lis (GSI) for the linguistic improvement of the manuscript.

- Krämer M, Durante M. Ion beam transport calculations and treatment plans in particle therapy. *Eur Phys J D* (2010) 60:195–202. doi:10.1140/epjd/e2010-00077-8
- Dreher C, Habermehl D, Ecker S, Brons S, El-Shafie R, Jäkel O, et al. Optimization of carbon ion and proton treatment plans using the raster-scanning technique for patients with unresectable pancreatic cancer. *Radiother Oncol* (2015) 10:850–860. doi:10.1186/s13014-015-0538-x
- Toftgaard J, Petersen JP, Bassler N. PyTRiP—a toolbox and gui for the proton/ion therapy planning system trip. *J Phys: Conf Ser* (2014) 489:012045. doi:10.1088/1742-6596/489/1/012045
- Ringbæk TP, Weber U, Santiago A, Iancu G, Wittig A, Grzanka L, et al. Validation of new 2d ripple filters in proton treatments of spherical geometries and non-small cell lung carcinoma cases. *Phys Med Biol* (2018) 62:245020. doi:10.1088/1361-6560/aaede9
- Ringbæk TP, Weber U, Santiago A, Simeonov Y, Fritz P, Krämer M, et al. Dosimetric comparisons of carbon ion treatment plans for 1d and 2d ripple filters with variable thicknesses. *Phys Med Biol* (2016) 61:4327. doi:10.1088/0031-9155/61/11/4327
- Bassler N, Hansen DC, Lühr A, Thomsen B, Petersen JP, Sobolevsky N. SHIELD-HIT12A—a Monte Carlo particle transport program for ion therapy research. *J Phys Conf* (2014) 489:012004. doi:10.1088/1742-6596/489/1/012004
- [Dataset] doi:10.5281/zenodo.4008066.Zenodo.org (2019)
- [Dataset] doi:10.17632/6jh3m9xtjx.1. Mendeley link (2019)
- [Dataset]MK. *Trip98 online manual*. Available from: <http://bio.gsi.de/DOCS/trip98.html> (2009)
- Schneider W, Bortfeld T, Schlegel W. Correlation between CT numbers and tissue parameters needed for Monte Carlo simulations of clinical dose distributions. *Phys Med Biol* (2000) 45:459–78. doi:10.1088/0031-9155/45/2/314
- Journal of the ICRU prescribing, recording and reporting proton-beam therapy (2007) Technical Report, Bethesda, MA: International Commission on Radiation Units and Measurements. Vol 7 No 2 (2007). Report 78.
- Schlegel U, Kraft G. Design and construction of a ripple filter for a smoothed depth dose distribution in conformal particle therapy. *Phys Med Biol* (1999) 44:2765–75. doi:10.1088/0031-9155/44/11/306
- Gemmel A, Hasch B, Ellerbrock M, Weyrather WK, Krämer M. Biological dose optimization with multiple ion fields. *Phys Med Biol* (2008) 53:6991–7012. doi:10.1088/0031-9155/53/23/022
- Scholz M, Kellerer AM, Kraft-Weyrather W, Kraft G. Computation of cell survival in heavy ion beams for therapy. *Radiat Environ Biophys* (1997) 36:59–66. doi:10.1007/s004110050055

**Conflict of Interest:** The authors declare that the research was conducted in the absence of any commercial or financial relationships that could be considered as a potential conflict of interest.

Copyright © 2020 Ringbæk, Santiago, Grzanka, Baumann, Flatten, Engenhart-Cabillic, Bassler, Zink and Weber. This is an open-access article distributed under the terms of the Creative Commons Attribution License (CC BY). The use, distribution or reproduction in other forums is permitted, provided the original author(s) and the copyright owner(s) are credited and that the original publication in this journal is cited, in accordance with accepted academic practice. No use, distribution or reproduction is permitted which does not comply with these terms.